Amplitude vs intensity Bayesian despeckling in the wavelet domain for SAR images

Amplitude vs Intensity Bayesian Despeckling in the Wavelet Domain for SAR Images

Tiziano Bianchi[a], Fabrizio Argenti[b], Alessandro Lapini[b], Luciano Alparone[b]

Corresponding author: Tiziano Bianchi, tel. +39 011 0904070, fax +39 011 0904099, e-mail: tiziano.bianchi@polito.it

[a] *Dept. of Electronics & Telecommunications, Politecnico di Torino Corso Duca degli Abruzzi, 24 - 10129 Torino, Italy*
[b] *Dept. of Information Engineering, University of Florence Via Santa Marta 3, 50139 Florence, Italy*

Abstract

In this paper, the problem of despeckling SAR images when the input data is either an intensity or an amplitude signal is revisited. State-of-the-art despeckling methods based on Bayesian estimators in the wavelet domain, recently proposed in the literature, are taken into consideration. First, how these methods proposed for one format (e.g., intensity) can be adapted to the other format (e.g., amplitude) is investigated. Second, the performance of such algorithms in both cases is analyzed. Experimental results carried out on simulated speckled images and on true SAR data are presented and discussed in order to assess the best strategy. From these results, it can be observed that filtering in the amplitude domain yields better performances in terms of objective quality indexes, such as preservation of structural details, as well as in terms of visual inspection of the filtered SAR data.

Keywords: Despeckling, intensity and amplitude SAR images, wavelet transform, Bayesian estimation.

1. Introduction

Speckle noise is a granular disturbance that degrades images acquired with active coherent systems. SAR, ultrasound sensors and sonar are examples of systems that produce data affected by speckle. Since image analysis may be

impaired by speckle, a pre-processing stage is commonly needed to diminish its effect (despeckling).

The acquisition instrument produces a radiation and captures the signals reflected from a small area of the imaged scene. Due to the presence of several scatterers within the resolution cell, the received signal is the sum of waves with a random phase so that the output from both the in-phase and the quadrature channels can be modelled as Gaussian variables. The acquired datum is a complex variable and the information is contained in the modulus (amplitude format, or AF) or in the squared modulus (intensity format, or IF) of this variable. When the images are visualized, the complex data can not be represented and the AF is commonly used. The phases induced by the different scatterers, however, introduce also a random variation on the information signal that can be modeled as a multiplicative noise u for both cases, AF and IF [1]. When this model applies, the noise is termed *fully developed* speckle. The distribution of u is an exponential probability density function (pdf) in the IF case and a Rayleigh pdf in the AF case [2].

In order to improve the quality of the acquired images, independent adjacent samples are averaged so that the variance of the speckle is reduced at the price of a resolution degradation (multi-look processing). If the average is taken over L samples of the single-look intensity image, then the speckle affecting the intensity of the multi-look datum is distributed according to a $\Gamma(L, L)$ pdf, whereas its square root is distributed according to a Nakagami distribution [3]. If amplitudes of the single-look image are averaged, the pdf of the speckle can not be expressed in a closed form, even though its moment can be computed.

The knowledge of the pdf of the speckle is fundamental in the formulation of despeckling filters based on Bayesian estimation that attempt to extract the noise-free reflectivity from a speckled observation [4, 5] as well as for other tasks, e.g., SAR imagery segmentation [6].

Recently, several despeckling methods have been proposed based on a multiresolution analysis, such as the wavelet transform. Despeckling in the wavelet domain is carried out by taking the wavelet decomposition of the observed sig-

nal, by estimating the speckle-free wavelet coefficients, and by reconstructing the filtered image using the inverse DWT (IDWT) applied to the despeckled coefficients. The wavelet transform may be either maximally decimated or redundant, even though the latter approach has several benefits for denoising applications, thanks to the shift-invariance property, since it significantly reduces structured artifacts [7].

When Bayesian methods are applied in the transformed domain, the pdf of the wavelet coefficients is needed. A statistical analysis of the coefficients belonging to a whole subband of the wavelet tranform has induced researchers to propose highly peaked distributions, such as the Laplacian or the generalized Gaussian (GG) pdf. In order to make Bayesian methods properly work, however, the pdf of coefficients should be computed locally, i.e., in a restricted neighbourhood of the pixel to be processed. Since a single realization of the imaged scene is usually available, assessing the validity of an hypothesized pdf is not possible from few data samples. Hence, a given pdf is "conjectured" to be valid and its parameters are derived from some statistical indexes (e.g., moments and cumulants) locally estimated.

Methods for Bayesian despeckling in the wavelet domain have been proposed, for instance, in [8, 9, 10, 11, 12, 13, 14, 15] for the case of SAR data and in [16, 17, 18, 19, 20] for the case of ultrasound and sonar data. Although the above methods are based on different models of the wavelet coefficients, a common feature is that they consider only intensity images. However, very often the modeling of the wavelet coefficients is not directly related to the actual distribution of the speckle, i.e., on the format of the SAR image. For example, in [11] wavelet coefficients are modeled by a very flexible generalized Gaussian model, requiring only the knowledge of the moments of the involved variables. To the best of our knowledge, there is no study in the literature assessing whether it is more convenient to filter wavelet coefficients of intensity or amplitude images.

The aim of this paper is twofold: first, despeckling methods based on Bayesian estimation in the wavelet domain are revisited and a unique formulation is given for the intensity and amplitude formats; second, the different methods are com-

pared by assessing their performances on both true SAR images and synthetically speckled test images - according to the models valid for AF and IF, either in the single-look or in the multi-look case - in order to determine the best filtering strategy.

The paper is organized as follows. In Section 2, the signal model and the pdfs of the wavelet coefficients of the signal and of the noise component are discussed. In Section 3, some Bayesian despeckling methods based on the wavelet transform and proposed for intensity signals are revisited and their application to amplitude signals is discussed. In Section 4, some experimental results carried out on synthetically speckled images as well as on true SAR images are presented in order to compare amplitude vs intensity despeckling methods. Some conclusions are drawn in Section 5.

2. Signal model

For the simplicity's sake, the model is formulated in one dimension. It is assumed that the available data are real and are given by

$$g(n) = f(n) \cdot u(n). \tag{1}$$

In this expression, $f(n)$ and $g(n)$ are the noise-free reflectivity and the observed signal, respectively. They can be in either amplitude or intensity format. The random variable $u(n)$ represents the fully developed speckle noise. We assume that $u(n)$ is unit-mean, uncorrelated and independent from $f(n)$ [21, 22, 23].

The multiplicative model in (1) can be translated into an additive one as follows:

$$\begin{aligned} g(n) &= f(n) + f(n) \cdot (u(n) - 1) = f(n) + f(n) \cdot u'(n) \\ &= f(n) + v(n). \end{aligned} \tag{2}$$

The mean of $u'(n) = u(n) - 1$ is zero and its pdf is directly derived from that of $u(n)$. The term $v(n)$ is signal-dependent and accounts for speckle disturbance.

2.1. Undecimated Wavelet Transform

The additive model in (2) is very convenient for modeling the wavelet coefficients of the observed signal. We will use the notation $A_f^{[j]}(n)$ and $W_f^{[j]}(n)$ to denote the *approximation* and the *detail* (or *wavelet*) coefficients, respectively, of the signal f at the jth level of the decomposition, whereas n is the spatial index. Unlike the maximally decimated DWT [24], undecimated DWT (UDWT) is considered here, where downsamplers and upsamplers are omitted from the analysis and synthesis stage, respectively.

It can be easily shown [8, 9] that the undecimated approximation and wavelet coefficients can be obtained by filtering the original signal by means of the following *equivalent filters*

$$\begin{aligned} H_{eq,l}^{[j]}(z) &= \prod_{m=0}^{j-1} H_0(z^{2^m}), \\ H_{eq,h}^{[j]}(z) &= \left[\prod_{m=0}^{j-2} H_0(z^{2^m})\right] \cdot H_1(z^{2^{j-1}}) \end{aligned} \tag{3}$$

where $H_0(z)$ and $H_1(z)$ denote the lowpass and highpass filters of the wavelet transform, respectively.

Since the wavelet transform is linear, from equation (2) we have

$$A_g^{[j]}(n) = A_f^{[j]}(n) + A_v^{[j]}(n), \tag{4}$$

$$W_g^{[j]}[n] = W_f^{[j]}(n) + W_v^{[j]}(n). \tag{5}$$

In the following, we will consider only the wavelet coefficients, i.e., the relationship in equation (5). Moreover, since filtering will be applied to each subband separately, to simplify the notation we will drop the superscript $[j]$. Whenever it does not create ambiguity, also the spatial index n will be omitted and we will denote with $h[n]$ a generic equivalent wavelet filter.

2.2. Probability Density Functions

Bayesian estimation in the wavelet domain relies on the pdfs of W_f and W_v, which in turn depend on the distributions of the speckle u and of the

reflectivity f. In the following, we will briefly review the probability density functions commonly used to model the above signals.

2.2.1. Reflectivity

The pdf of f depends on the imaged scene and is difficult to estimate, even though several models exist based on the heterogeneity of the underlying area (uniform, textured, etc.) [23, 25, 26]. The solutions considered in this paper do not rely on a particular distribution of f, hence such models are not further investigated.

2.2.2. Speckle

The pdf of the speckle process u depends on the specific format of the signal [3]. For IF single-look images the pdf of u is exponential, whereas for multi-look images the pdf of u becomes a $\Gamma(L, L)$, given by

$$p_U(u) = \frac{L^L}{\Gamma(L)} u^{L-1} e^{-uL}. \tag{6}$$

For AF single-look images the pdf of u is a unit mean Rayleigh pdf, given by

$$p_U(u) = \frac{\pi u}{2} e^{-\frac{\pi u^2}{4}} \tag{7}$$

whereas for AF multi-look images u is distributed according to the average of L independent unit mean Rayleigh variables and its pdf can not be expressed in a closed form.

Sometimes, it is convenient to consider also the squared root of an IF (SIF) image, which can be considered as an alternative amplitude format. In this case, for a SIF single-look image u is Rayleigh distributed with mean equal to $\sqrt{\pi}/2$, whereas for SIF multi-look images the pdf of u is a Nakagami pdf given by

$$p_U(u) = \frac{2L^L}{\Gamma(L)} u^{2L-1} e^{-u^2 L}. \tag{8}$$

For SIF images the mean of u is different from one, however the model in (1) is still valid if we rescale the square root of the intensity by a factor $\mu_{\mathrm{SIF}}(L) = L^{-\frac{1}{2}}\Gamma(L)/\Gamma(L+\frac{1}{2})$. It is worth noting that single-look AF and rescaled SIF

images have identical distribution, whereas multi-look AF and rescaled SIF images have different distributions and must be considered different formats. In the following, with SIF images we will always refer to rescaled SIF images.

2.2.3. Wavelet Coefficients

As noticed by Mallat in his seminal paper [24], the pdf of the wavelet coefficients can be approximated by a family of unimodal distributions that can be efficiently modeled by a generalized Gaussian (GG) pdf. A zero-mean GG pdf depends only on two parameters and its expression is given by

$$p_{W_X}(W_x) = \left[\frac{\nu_{W_X} \cdot \eta(\nu_{W_X}, \sigma_{W_X})}{2 \cdot \Gamma(1/\nu_{W_X})}\right] e^{-[\eta(\nu_{W_X}, \sigma_{W_X}) \cdot |W_x|]^{\nu_{W_X}}} \tag{9}$$

where Γ is the Gamma function, σ_{W_X} is the standard deviation of the distribution, ν_{W_X} is a *shape factor*, and $\eta(\nu_{W_X}, \sigma_{W_X})$ is given by

$$\eta(\nu_{W_X}, \sigma_{W_X}) = \frac{1}{\sigma_{W_X}} \left[\frac{\Gamma(3/\nu_{W_X})}{\Gamma(1/\nu_{W_X})}\right]^{1/2}. \tag{10}$$

As particular cases, the GG pdf includes both the Laplacian and the Gaussian pdfs, for $\nu = 1$ and $\nu = 2$, respectively.

Assessing the validity of a specific pdf for the wavelet coefficients, however, is not a simple task. The analysis of the histogram of the coefficients of a whole subband yields "global" information about the distribution, whereas, due to the nonstationarity of the image, "local" information should be pursued instead. Spatially adaptive methods make the "conjecture" that a given pdf is valid locally and try to compute its parameters from the few data available in a window of the signal. The most viable solution for achieving the pdf parameters is based on the estimation of few spatially varying statistical indexes - for example, cumulants and moments - of the data in a small area of the image.

The local GG model has been successfully used in [11, 12] to model the wavelet coefficients of IF images, whereas local Gaussian and Laplacian models have been used in [9, 14], again considering IF images. However, in principle such models do not depend on the IF assumptions and can be also used to model the wavelet coefficients of AF and SIF images.

3. Bayesian despeckling in the wavelet domain

In the last decade, several despeckling methods based on Bayesian estimation in the DWT or in the undecimated DWT domain have been proposed. The methods differ each other for the choice of the estimation criterion used to achieve the despeckled coefficients and for the modelling of the data in the wavelet domain.

Bayesian estimation requires the knowledge of the pdfs of the wavelet coefficients relative to the signal of interest (the reflectivity), also referred to as *prior* pdf, and to the noise component.

As to the knowledge about u in (2), it will be shown that to achieve the solution of the despeckling problem only the moments of u are necessary. In the following, some despeckling methods are reviewed and the necessary information that is needed to achieve the solution is provided for the IF, AF, and SIF signals.

3.1. LMMSE filter

The linear minimum mean square error (LMMSE) criterion is the simplest Bayesian despeckling filter. It is the optimal solution when both signal and noise components have a Gaussian pdf. The expression of the estimated despeckled coefficients is given by [9]

$$\hat{W}_f(n) = \frac{E[W_g^2(n)] - E[W_v^2(n)]}{E[W_g^2(n)]} W_g(n) \tag{11}$$

and depends only on the second-order moment of $W_v(n)$ (besides to the observable variable $W_g(n)$ and its second moment).

3.2. MAP filters

Unlike the LMMSE case, where only the moments of the involved random processes are needed, in general Bayesian filtering needs a precise knowledge of their pdf. By using Bayes' rule, it can be demonstrated that the maximum a-posteriori probability (MAP) estimator of W_f is given by the solution of the

following problem [8, 11]

$$\begin{aligned}\hat{W}_f &= \arg\max_{W_f}\ p_{W_F|W_G}(W_f|W_g) \\ &= \arg\max_{W_f}\ p_{W_V|W_F}(W_g - W_f|W_f)p_{W_F}(W_f),\end{aligned} \tag{12}$$

so that it depends on the knowledge of p_{W_F} and $p_{W_V|W_F}$. In the following, we will consider two solutions based on the pdf models of Section 2.2.3.

3.2.1. Laplacian-Gaussian

In [14], a despeckling method based on the MAP solution and on the assumptions that the pdf of W_f is Laplacian and the pdf of W_v is Gaussian has been presented (MAP-LG). The method has the advantage that a closed-form solution exists and is given by

$$\hat{W}_f(n) = \begin{cases} W_g(n) - \frac{\sqrt{2}E[W_v^2(n)]}{\sqrt{E[W_f^2(n)]}} & \text{if } W_g(n) > \frac{\sqrt{2}E[W_v^2(n)]}{\sqrt{E[W_f^2(n)]}} \\ W_g(n) + \frac{\sqrt{2}E[W_v^2(n)]}{\sqrt{E[W_f^2(n)]}} & \text{if } W_g(n) < -\frac{\sqrt{2}E[W_v^2(n)]}{\sqrt{E[W_f^2(n)]}} \\ 0 & \text{elsewhere.} \end{cases} \tag{13}$$

Due to the simple form of the involved pdfs, only the second-order moments of $W_f(n)$ and of $W_v(n)$ are necessary to achieve the solution.

3.2.2. Generalized Gaussian

In [11] a despeckling method based on the MAP criterion and on the GG assumption has been presented (MAP-GG). The despeckled coefficients are estimated as the solution of

$$\begin{aligned}\hat{W}_f(n) = \arg\min_{W_f(n)} \big[&\left(\eta_{W_f(n)}|W_f(n)|\right)^{\nu_{W_f(n)}} \\ &+ \left(\eta_{W_v(n)}|W_g(n) - W_f(n)|\right)^{\nu_{W_v(n)}}\big]\end{aligned} \tag{14}$$

where the shape factors can be estimated by inverting

$$\frac{E\left[X^2\right]}{\sqrt{E\left[X^4\right]}} = \frac{\Gamma(3/\nu_X)}{\sqrt{\Gamma(1/\nu_X)\Gamma(5/\nu_X)}} \tag{15}$$

where X is either $W_f(n)$ or $W_v(n)$. As can be seen, the second and fourth-order moments of both $W_f(n)$ and $W_v(n)$ are necessary to solve the problem.

3.3. Moments of Wavelet Coefficients

All of the above solutions are based on the knowledge of some moments of either $W_f(n)$ or $W_v(n)$. In general, such moments can be expressed as a function of the moments of the observed variables $g(n)$ and $W_g(n)$, the equivalent filter $h(n)$, and the moments of the speckle variables u and u'. Several expressions have been proposed in the literature. In the following, we report the exact expression derived in [12]:

$$E\left[W_v^2(n)\right] = \frac{\mu_{u'}^{[2]}}{\mu_u^{[2]}} E\left[M_g^{[2]}(n)\right] \tag{16}$$

$$E\left[W_f^2(n)\right] = E\left[W_g^2(n) + \left(\frac{1}{\mu_u^{[2]}} - 1\right) M_g^{[2]}(n)\right] \tag{17}$$

$$\begin{aligned} E\left[W_v^4(n)\right] =& E\left[3\left(\frac{\mu_{u'}^{[2]}}{\mu_u^{[2]}}\right)^2 \left(M_g^{[2]}(n)\right)^2 \right. \\ & \left. + \left(\frac{\mu_{u'}^{[4]}}{\mu_u^{[4]}} - 3\left(\frac{\mu_{u'}^{[2]}}{\mu_u^{[2]}}\right)^2\right) M_g^{[4]}(n)\right] \end{aligned} \tag{18}$$

$$\begin{aligned} E[W_f^4(n)] =& E\left[W_g^4(n) + \left(\frac{6}{\mu_u^{[2]}} - 6\right) W_g^2(n) M_g^{[2]}(n) \right. \\ & + \left(\frac{3}{\left(\mu_u^{[2]}\right)^2} - \frac{6}{\mu_u^{[2]}} + 3\right) \left(M_g^{[2]}(n)\right)^2 \\ & + \left(\frac{4}{\mu_u^{[3]}} - \frac{12}{\mu_u^{[2]}} + 8\right) W_g(n) M_g^{[3]}(n) \\ & \left. + \left(\frac{1}{\mu_u^{[4]}} - \frac{4}{\mu_u^{[3]}} - \frac{3}{\left(\mu_u^{[2]}\right)^2} + \frac{12}{\mu_u^{[2]}} - 6\right) M_g^{[4]}(n)\right] \end{aligned} \tag{19}$$

where we define $\mu_u^{[k]} = E[u^k]$ and $M_g^{[k]}(n) = \sum_i h^k(i) g^k(n-i)$. In practice, the moments of the observed variables can be estimated using local averages, whereas the moments of u and u' can be computed according to the number of look L and the image format, as specified in the next subsection.

3.4. Moments of Speckle Variables

The solutions derived so far are not based on a specific image format. As long as the input signal obeys the model in (1), the filters defined by (11), (13),

and (14), based on the moments given in (16)-(19), can be applied to IF, AF, or rescaled SIF images, provided that the correct moments of the speckle variables are used. In the following, we will derive the expression of the moments of u according to the number of look L and the image format. As to the moments of u', they can be easily derived from the moments of u as follows:

$$\begin{aligned}
\mu_{u'}^{[1]} &= 0 \\
\mu_{u'}^{[2]} &= \mu_u^{[2]} - 1 \\
\mu_{u'}^{[3]} &= \mu_u^{[3]} - 3\mu_u^{[2]} + 2 \\
\mu_{u'}^{[4]} &= \mu_u^{[4]} - 4\mu_u^{[3]} + 6\mu_u^{[2]} - 3
\end{aligned}$$

3.4.1. Intensity

When u is distributed according to (6), its moments can be expressed as [27]

$$\mu_u^{[m]}(L) = \frac{\Gamma(L+m)}{\Gamma(L)} \frac{1}{L^m}. \tag{20}$$

3.4.2. Amplitude

In the case of single-look AF signals, u has a Rayleigh pdf given by (7) and its moments can be expressed as

$$\mu_u^{[m]}(1) = \left(\frac{4}{\pi}\right)^{\frac{m}{2}} \Gamma\left(1 + \frac{m}{2}\right). \tag{21}$$

When u is the average of L i.i.d. variables distributed according to (7), it can be shown (see Appendix A) that its moments can be expressed by

$$\mu_u^{[1]}(L) = 1 \tag{22}$$

$$\mu_u^{[2]}(L) = \frac{1}{\pi L}[4 + \pi(L-1)] \tag{23}$$

$$\mu_u^{[3]}(L) = \frac{1}{\pi L^2}[6 + 12(L-1) + \pi(L-2)(L-1)] \tag{24}$$

$$\mu_u^{[4]}(L) = \frac{1}{\pi^2 L^3}\big[32 + 48(L-1) + 24\pi(L-1)^2 \tag{25}$$

$$+ \pi^2(L-3)(L-2)(L-1)\big] \tag{26}$$

$$\tag{27}$$

3.4.3. Square Root of Intensity

If we denote as $\tilde{u}$ the square root of an intensity speckle process, distributed as (8), its moments are given by [3]

$$\mu_{\tilde{u}}^{[m]}(L) = \frac{\Gamma\left(L+\frac{m}{2}\right)}{\Gamma(L)}\frac{1}{L^{\frac{m}{2}}}. \tag{28}$$

Hence, the moments of u for a rescaled SIF signal can be obtained as

$$\mu_{u}^{[m]}(L) = \frac{\mu_{\tilde{u}}^{[m]}(L)}{\left(\mu_{\tilde{u}}^{[1]}(L)\right)^{m}} = \frac{\Gamma(L)^{m-1}\Gamma\left(L+\frac{m}{2}\right)}{\Gamma\left(L+\frac{1}{2}\right)^{m}}. \tag{29}$$

3.5. Segmentation

Recent works on despeckling SAR images demonstrate that filtering performance is usually improved by applying different statistical models to different areas of the image. In [12], each wavelet plane is segmented according to the variance of the texture component of the signal into homogenous, heterogeneous, and highly heterogenous classes, and different GG parameters are used for each class. A similar approach is used in [14], where the homogenous classes are filtered through the MAP-LG filter and the heterogenous classes are filtered through the LMMSE filter. In the following, we will refer to the above filters as MAP-GG-S and MAP-LG-S, respectively.

According to the model proposed in [12] (see equations (24)-(25) in [12]), the variance of the texture component can be expressed again as a function of the moments of the observed signal g, the equivalent filter coefficients h, and the variance of the speckle variable u. Hence, even MAP-GG-S and MAP-LG-S filters can be applied irrespective of the format of the underlying signal, provided that the correct expression of σ_u^2 is used in the computation of the variance of the texture component.

4. Experimental Results

The performances of the different filters on different image formats have been assessed on both simulated images and true SAR images. As to simulated

(a) (b) (c)

Figure 1: Original images: (a) "Lena"; (b) "Barbara"; (c) "San Francisco".

images, the performances are measured by computing the peak-signal-to-noise ratio (PSNR) and the mean structural similarity index (MSSIM) between the original and the filtered images. The PSNR is defined as

$$\mathrm{PSNR} = 10 \log_{10} \left(\frac{I_{peak}^2}{E[(\hat{I} - I)^2]} \right) \tag{30}$$

where I is the original image, $\hat{I}$ is the filtered image, and I_{peak} is the peak value (for 8-bit images, we assume $I_{peak} = 255$). The PSNR, as well as closely related metrics like the mean square error between the original and the filtered images, have been often used to assess the performance of despeckling applications [11, 28]. The MSSIM is a measure of degradation of structural information and it is defined as [29]

$$\mathrm{MSSIM} = E \left[\frac{(2\mu_I \mu_{\hat{I}} + C_1)(2\sigma_{I\hat{I}} + C_2)}{(\mu_I^2 + \mu_{\hat{I}}^2 + C_1)(\sigma_I^2 + \sigma_{\hat{I}}^2 + C_2)} \right] \tag{31}$$

where μ_I, σ_I^2, $\mu_{\hat{I}}$, $\sigma_{\hat{I}}^2$, and $\sigma_{I\hat{I}}$ are the local mean, variance, and covariance of the original and filtered images, whereas C_1 and C_2 are two suitable constants. Since we want to avoid the comparison to be biased by the the format in which the measures are taken, we consider both I and $\hat{I}$ in the amplitude format; that is, for IF we use $I = \sqrt{f}$ and $\hat{I} = \sqrt{\hat{f}}$, while for both SIF and AF we use $I = f$ and $\hat{I} = \hat{f}$.

Moreover, as a no-reference index of the quality of the filtered images, we report the sample mean and the sample variance of the ratio between the observed

and the filtered images, defined as

$$\hat{u} = \frac{g}{\hat{f}}. \tag{32}$$

The analysis of the ratio image is generally considered an efficient global filtering test [23, 30, 5]. For a good despeckling filter, $\hat{u}$ should be as close as possible to the speckle process u and we should obtain $\mu_{\hat{u}} = 1$, i.e., the filter should preserve the radiometric properties of the observed scene, and $\sigma^2_{\hat{u}} = \sigma^2_u$. In the case of IF and SIF images, the statistics have been evaluated on intensity values and we have $\sigma^2_u = 1/L$. In the case of AF images, the statistics have been evaluated on amplitude values and we have $\sigma^2_u = (4-\pi)/(\pi L)$. For a better evaluation of the estimated values, in all the following tables the normalized values $\sigma^2_u \cdot L$ or $\sigma^2_u \cdot (\pi L)/(4-\pi)$ are reported. Since there is no need of using the original image as a reference, the above indexes can be used for both simulated and true SAR images.

For all tested filters, the biorthogonal 9/7 wavelets [31] have been used, with a four level decomposition.

4.1. Simulated Images

We considered three 8-bit 512×512 optical images, "Lena", "Barbara", and "San Francisco", corrupted by synthetic speckle generated according to the models in (6)-(8) considering different number of look L. The original images are shown in Fig. 1. In Tables 1–3, we report the results obtained in the case of IF and SIF images, whereas in Tables 4–6 we report the results obtained in the case of AF images.

The results clearly show that filtering SIF images outperforms filtering IF images. For each image and for each number of look, all filters yield a higher PSNR when operating in the SIF domain. For example, the MAP-GG filter gains about 0.6 dB in PSNR for the single-look "Lena" and "Barbara" images and about 0.9 dB in PSNR for the single-look "San Francisco" image. As to the MSSIM, in the case of the "Lena" image we have very similar values for both formats, whereas in the case of the "Barbara" and"San Francisco" images,

the MSSIM is slightly better for SIF, indicating that filtering the square root of intensity neither introduces artifacts nor alters structural information. The above results are also confirmed by inspecting the values of $\mu_{\hat{u}}$ and $\sigma^2_{\hat{u}}$ for the different filters: the values of $\mu_{\hat{u}}$ are always very similar for both formats; the values of $\sigma^2_{\hat{u}}$, especially for the MAP-GG and MAP-GG-S filters, in the case of "Barbara" and"San Francisco" are closer to the theoretical variance of the speckle for SIF, whereas in the case of "Lena" are slightly better for IF.

In the case of AF images, we can see that all filters obtain results very close to those obtained on SIF images. Also the values of the statistical parameters $\mu_{\hat{u}}$ and $\sigma^2_{\hat{u}}$ confirm a good performance of the filters for this kind of images, especially in the case of the MAP-GG filter, which yields a $\sigma^2_{\hat{u}}$ quite close to the theoretical value on all images. It is interesting to note that the LMMSE filter exhibits a bias irrespective of the SAR image format, indicating that Gaussian modeling of wavelet coefficients is not adequate even in the case of amplitude and square root of intensity signals.

4.2. True SAR Images

Results on true SAR data have been assessed by using two 16 bit 512×512 COSMO-SkyMed 1-look X-HH images showing the area near the airport of Firenze, Italy. For showing results on intensity multilooked data, two corresponding 4-look 256×256 intensity images have been obtained by averaging four neighbouring pixels and downsampling the intensity of the 1–look images. Furthermore, by means of the same procedure, two corresponding 4-look 256×256 amplitude images have been obtained from the amplitude of the 1–look images. The 1-look "COSMO-SkyMed" images are shown in Fig. 2.

The statistics $\mu_{\hat{u}}$ and $\sigma^2_{\hat{u}}$ of the extracted speckle in the three considered image formats and for all the considered filters have been evaluated on two different homogeneous areas, denoted as "A" and "B" in Fig. 2.

The results for the IF and SIF domains, reported in Table 7, indicate that the despeckling performance of both approaches is very similar on areas affected by fully developed speckle. All filters, apart from the LMMSE one, are virtually

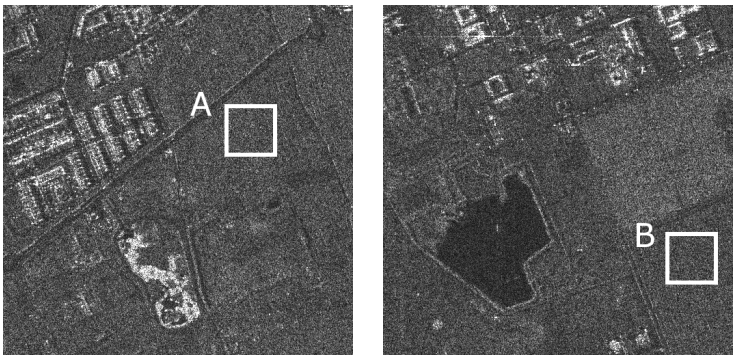

Figure 2: 1-look "COSMO-SkyMed" images used in the experiments.

unbiased irrespective of the image format. Also, the variance of the estimated speckle noise is quite close to the theoretical value, with very little differencies between IF and SIF. Namely, IF appears to achieve a slightly better $\sigma^2_{\hat{u}}$ for 1-look images, whereas SIF achieve slightly better results for 4–look images. In Table 8, the results for the 4–look image in the AF domain are shown. It is interesting to note that the indexes are very similar to those obtained for the 4–look SIF case, except for the LMMSE filter where a reduction of bias is observed in the AF domain.

For visual inspection, we propose the images obtained by applying the MAP-GG-S filter in the IF and SIF domains for the 1-look case (Fig. 3) and for the 4-look case (Fig. 4), as well as the images obtained by applying the same filter for the 4–look case in the AF domain (Fig. 5). From all the examples, it is apparent that filtering SIF or AF images is usually beneficial. As to homogeneous areas, the smoothing degree obtained by the filter, as well as the artifacts produced by the wavelet synthesis stage, are similar for all the proposed formats. Conversely, it is particularly evident that filtering SIF or AF images yields a better preservation of details, since it produces less artifacts near edges, high variance regions, and targets. From the comparison of 4–look SIF and AF images we can observe no appreciable differences between the despeckled images obtained from the two formats.

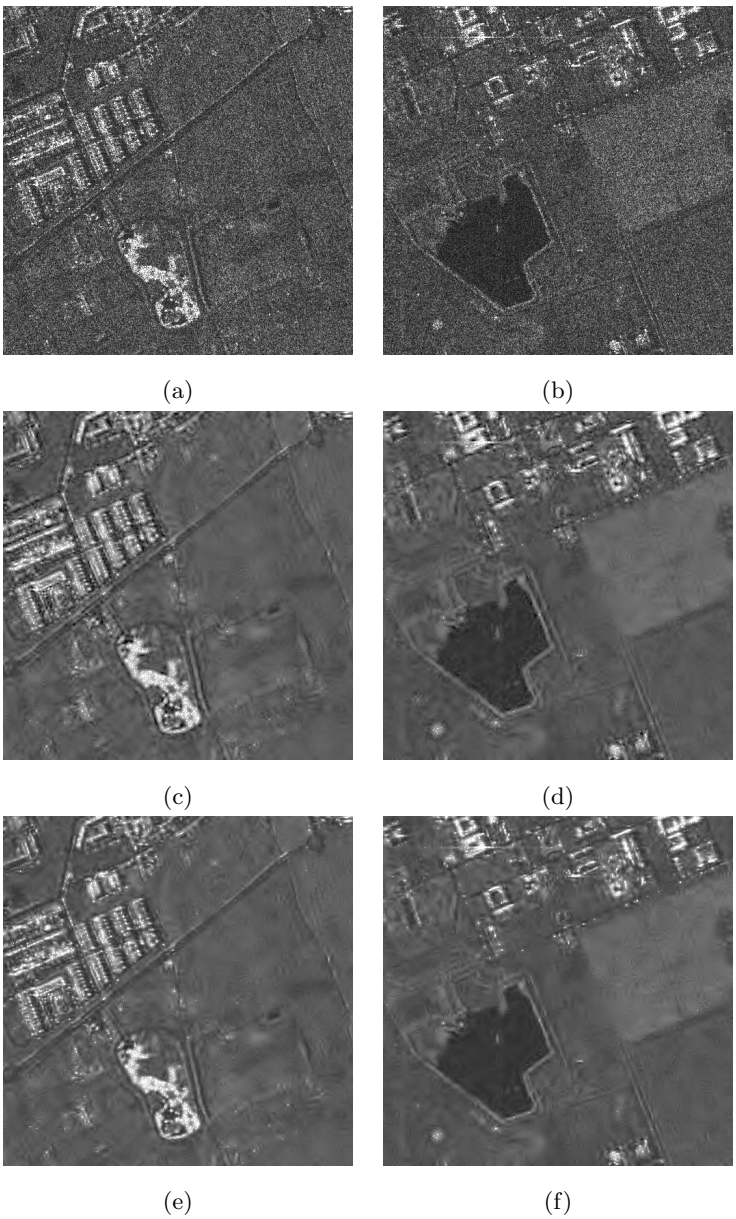

Figure 3: Example of despeckling of the 1-look "COSMO-SkyMed" images: (a)-(b) original; (c)-(d) MAP-GG-S filtered, IF; (e)-(f) MAP-GG-S filtered, SIF.

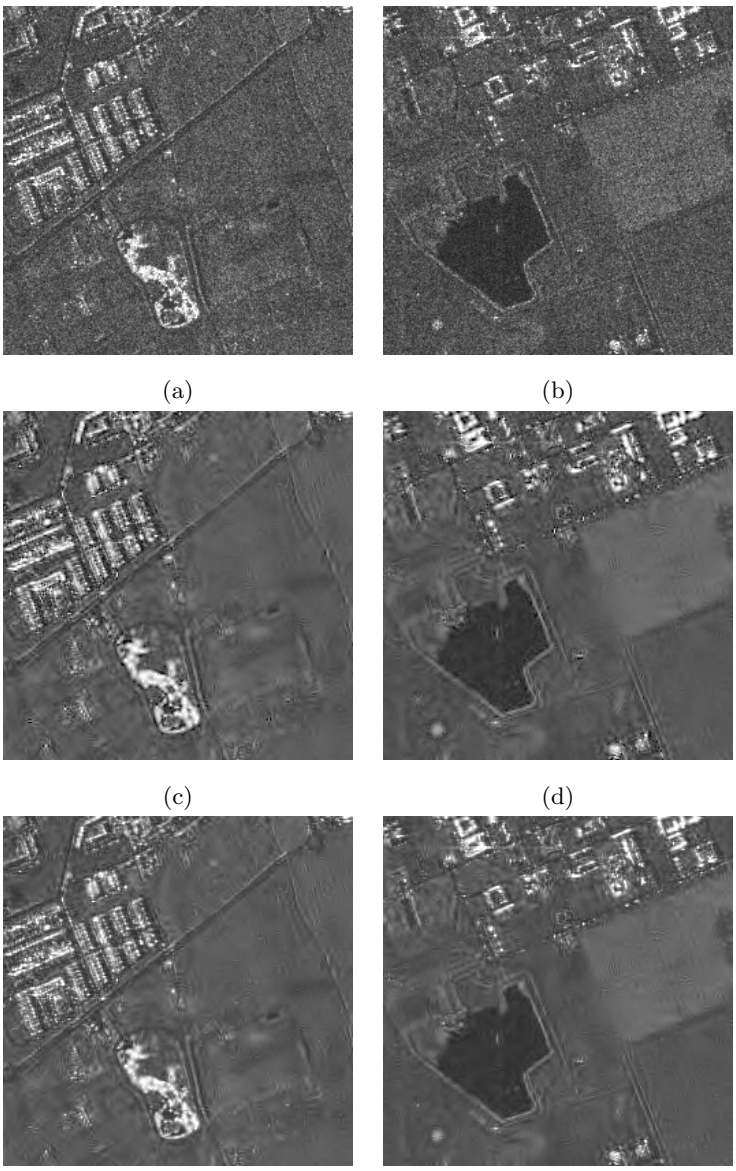

Figure 4: Example of despeckling of the 4-look intensity "COSMO-SkyMed" images: (a)-(b) original; (c)-(d) MAP-GG-S filtered, IF; (e)-(f) MAP-GG-S filtered, SIF.

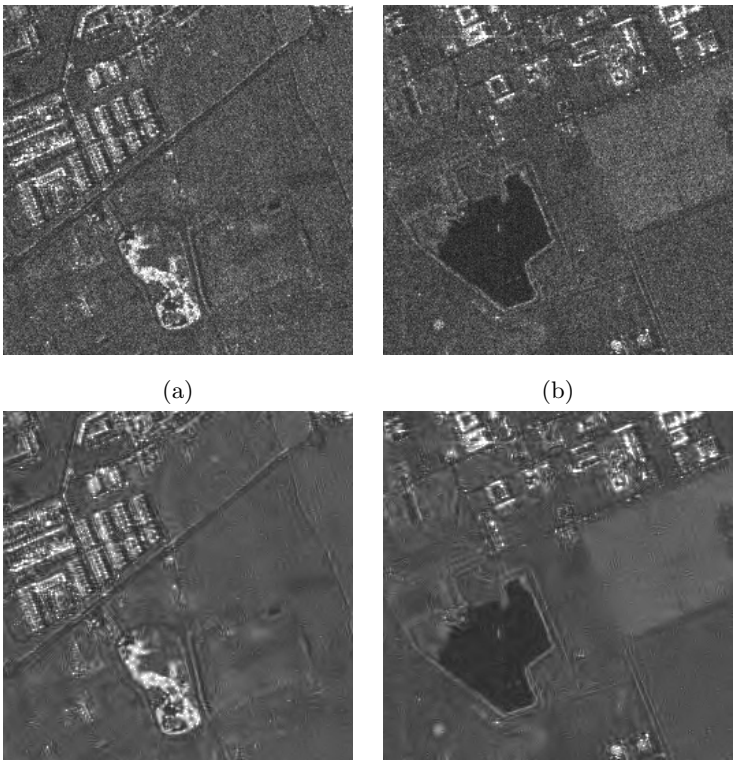

Figure 5: Example of despeckling of the 4-look amplitude "COSMO-SkyMed" images: (a)-(b) original; (c)-(d) MAP-GG-S filtered.

5. Conclusions

In this work, we have presented a study on despeckling images affected by multiplicative noise in either amplitude or intensity format. Bayesian despeckling algorithms in the wavelet domain have been considered. We have shown that a common framework for the despeckling problem can be setup for various formats - satisfying the multiplicative model - based on the computation of the moments of the speckle component. Such moments are derived for single-look and multi-look images. In the latter case, amplitude multi-look images can be obtained either averaging amplitude signals or taking the square root of the average of intensity signals. The experimental results have been carried out on both synthetically speckled images and on true SAR COSMO-SkyMed images.

The results obtained on synthetically degraded images show that a significant improvement of objective quality measures can be observed when the wavelet decomposition is applied on amplitude images. On the other hand, for both synthetically speckled and true SAR images, filtering either in the amplitude or in the intensity domain yields statistical parameters of the extracted speckle noise which are quite similar. For the MAP–GG and MAP–GG-S filters this is not surprising, since both filters already achieved almost optimal performance in the SIF case. Moreover, this fact indicates that, even though the domain of filtering may not significantly affect the global statistical performance of the filters, filtering in the amplitude domain yields a better preservation of structural details. The above observation is confirmed by the visual inspection of filtered SAR data, since images filtered in either SIF or AF domain show less artifacts in the presence of highly heterogenous areas.

The observed behaviour can be explained by a more effective modeling of the wavelet coefficients of amplitude SAR signals and a more robust estimation of the moments for the amplitude case. The above results also suggest that AF and SIF should be the preferred image formats when despeckling is performed in the wavelet domain, and that existing IF images should always be converted to SIF before processing with this kind of despeckling filters.

Appendix A. Derivation of Amplitude multi-look speckle moments

When u is the average of L i.i.d. variables r_i, $i = 1, \ldots, L$, distributed according to (7), its moments can be derived as follows:

$$\mu_u^{[1]}(L) = E\left[\frac{1}{L}\sum_i r_i\right] = \frac{1}{L}\sum_i E[r_i] = E[r] \tag{A.1}$$

$$\begin{aligned}\mu_u^{[2]}(L) &= E\left[\left(\frac{1}{L}\sum_i r_i\right)^2\right] \\ &= \frac{1}{L^2}\left(\sum_i E[r_i^2] + \sum_i \sum_{j\neq i} E[r_i]E[r_j]\right) \\ &= \frac{1}{L}E[r^2] + \frac{L-1}{L}E[r]^2\end{aligned} \tag{A.2}$$

$$\begin{aligned}\mu_u^{[3]}(L) =& E\left[\left(\frac{1}{L}\sum_i r_i\right)^3\right] \\ =& \frac{1}{L^3}\left(\sum_i E[r_i^3] + 3\sum_i \sum_{j\neq i} E[r_i^2]E[r_j]\right. \\ &\left. + \sum_i \sum_{j\neq i} \sum_{k\neq j\neq i} E[r_i]E[r_j]E[r_k]\right) \\ =& \frac{1}{L^2}E[r^3] + \frac{3(L-1)}{L^2}E[r^2]E[r] \\ &+ \frac{(L-2)(L-1)}{L^2}E[r]^3\end{aligned} \tag{A.3}$$

$$
\begin{aligned}
\mu_u^{[4]}(L) =& E\left[\left(\frac{1}{L}\sum_i r_i\right)^4\right] \\
=& \frac{1}{L^4}\left(\sum_i E[r_i^4] + 4\sum_i\sum_{j\neq i} E[r_i^3]E[r_j]\right. \\
&+3\sum_i\sum_{j\neq i} E[r_i^2]E[r_j^2] \\
&+6\sum_i\sum_{j\neq i}\sum_{k\neq j\neq i} E[r_i^2]E[r_j]E[r_k] \\
&\left.+\sum_i\sum_{j\neq i}\sum_{k\neq j\neq i}\sum_{h\neq k\neq j\neq i} E[r_i]E[r_j]E[r_k]E[r_h]\right) \\
=& \frac{1}{L^3}E[r^4] + \frac{4(L-1)}{L^3}E[r^3]E[r] + \frac{3(L-1)}{L^3}E[r^2]^2 \\
&+\frac{6(L-2)(L-1)}{L^3}E[r^2]E[r]^2 \\
&+\frac{(L-3)(L-2)(L-1)}{L^3}E[r]^4
\end{aligned}
\tag{A.4}
$$

where $E[r^m] = \mu_u^{[m]}(1)$. After some simple algebra, the moments result to be those expressed in (22).

References

[1] M. Tur, K. C. Chin, J. W. Goodman, When is speckle multiplicative?, Appl. Optics 21 (1982) 1157–1159.

[2] J. W. Goodman, Some fundamental properties of speckle, J. Opt. Soc. Amer. 66 (1976) 1145–1150.

[3] H. Xie, L. E. Pierce, F. T. Ulaby, Statistical properties of logarithmically transformed speckle, IEEE Trans. Geosci. Remote Sensing 40 (2002) 721–727.

[4] J.-S. Lee, I. Jurkevich, P. Dewaele, P. Wambacq, A. Oosterlinck, Speckle filtering of synthetic aperture radar images: a review, Remote Sensing Reviews 8 (1994) 313–340.

[5] R. Touzi, A review of speckle filtering in the context of estimation theory, IEEE Trans. Geosci. Remote Sensing 40 (2002) 2392–2404.

[6] E. Carvalho, D. Ushizima, F. Medeiros, C. Martins, R. Marques, I. Oliveira, SAR imagery segmentation by statistical region growing and hierarchical merging, Digital Signal Processing 20 (2010) 1365 – 1378.

[7] G. P. Nason, B. W. Silverman, The stationary wavelet transform and some statistical applications, in: A. Antoniadis, G. Oppenheim (Eds.), Wavelets and Statistics, volume 103 of *Lecture Notes Statist.*, Springer-Verlag, New York, 1995, pp. 281–299.

[8] S. Foucher, G. B. Bénié, J.-M. Boucher, Multiscale MAP filtering of SAR images, IEEE Trans. Image Processing 10 (2001) 49–60.

[9] F. Argenti, L. Alparone, Speckle removal from SAR images in the undecimated wavelet domain, IEEE Trans. Geosci. Remote Sensing 40 (2002) 2363–2374.

[10] S. Solbø, T. Eltoft, Homomorphic wavelet-based statistical despeckling of SAR images, IEEE Trans. Geosci. Remote Sensing 42 (2004) 711–721.

[11] F. Argenti, T. Bianchi, L. Alparone, Multiresolution MAP despeckling of SAR images based on locally adaptive generalized Gaussian pdf modeling, IEEE Trans. Image Processing 15 (2006) 3385–3399.

[12] T. Bianchi, F. Argenti, L. Alparone, Segmentation-based MAP despeckling of SAR images in the undecimated wavelet domain, IEEE Trans. Geosci. Remote Sensing 46 (2008) 2728–2742.

[13] M. Amirmazlaghani, H. Amindavar, A. Moghaddamjoo, Speckle suppression in SAR images using the 2-D GARCH model, IEEE Transactions on Image Processing 18 (2009) 250 – 259.

[14] F. Argenti, T. Bianchi, A. Lapini, L. Alparone, Fast MAP despeckling based on Laplacian-Gaussian modeling of wavelet coefficients, IEEE Geoscience and Remote Sensing Letters 9 (2012) 13 –17.

[15] B. Hou, X. Zhang, X. Bu, H. Feng, SAR image despeckling based on nonsubsampled shearlet transform, IEEE Journal of Selected Topics in Applied Earth Observations and Remote Sensing 5 (2012) 809 – 823.

[16] A. Achim, A. Bezerianos, P. Tsakalides, Novel Bayesian multiscale method for speckle removal in medical ultrasound images, IEEE Transactions on Medical Imaging, 20 (2001) 772 –783.

[17] S. Gupta, L. Kaur, R. Chauhan, S. Saxena, A versatile technique for visual enhancement of medical ultrasound images, Digital Signal Processing 17 (2007) 542 – 560.

[18] F. Chaillan, C. Fraschini, P. Courmontagne, Speckle noise reduction in SAS imagery, Signal Processing 87 (2007) 762 – 781.

[19] M. Bhuiyan, M. Ahmad, M. Swamy, Spatially adaptive thresholding in wavelet domain for despeckling of ultrasound images, IET Image Processing 3 (2009) 147 –162.

[20] A. Khare, M. Khare, Y. Jeong, H. Kim, M. Jeon, Despeckling of medical ultrasound images using Daubechies complex wavelet transform, Signal Processing 90 (2010) 428 – 439.

[21] V. S. Frost, J. A. Stiles, K. S. Shanmugan, J. C. Holtzman, A model for radar images and its application to adaptive digital filtering of multiplicative noise, IEEE Trans. Pattern Anal. Machine Intell. 4 (1982) 157–166.

[22] S. Madsen, Spectral properties of homogeneous and nonhomogeneous radar images, IEEE Transactions on Aerospace and Electronic Systems, AES-23 (1987) 583 –588.

[23] C. Oliver, S. Quegan, Understanding Synthetic Aperture Radar Images, Artech House, Boston, MA, 1998.

[24] S. Mallat, A theory for multiresolution signal decomposition: the wavelet representation, IEEE Trans. Pattern Anal. Machine Intell. PAMI-11 (1989) 674–693.

[25] A. Lopès, E. Nezry, R. Touzi, H. Laur, Structure detection and statistical adaptive speckle filtering in SAR images, Int. J. Remote Sensing 14 (1993) 1735–1758.

[26] A. C. Frery, H.-J. Muller, C. C. F. Yanasse, S. J. S. Sant'Anna, A model for extremely heterogeneous clutter, IEEE Trans. Geosci. Remote Sensing 35 (1997) 648–659.

[27] M. G. Kendall, A. Stuart, The Advanced Theory of Statistics, volume 1, Charles Griffin & Co., Ltd., London, UK, 4th edition, 1977.

[28] C.-A. Deledalle, L. Denis, F. Tupin, Iterative weighted maximum likelihood denoising with probabilistic patch-based weights, IEEE Transactions on Image Processing 18 (2009) 2661–2672.

[29] Z. Wang, A. Bovik, H. Sheikh, E. Simoncelli, Image quality assessment: from error visibility to structural similarity, IEEE Trans. Image Processing 13 (2004) 600 – 612.

[30] M. Walessa, M. Datcu, Model-based despeckling and information extraction from SAR images, IEEE Trans. Geosci. Remote Sensing 38 (2000) 2258–2269.

[31] I. Daubechies, Ten Lectures on Wavelets, volume 61 of *CBMS-NSF Reg. Conf. Series Appl. Math.*, SIAM, Philadelphia, PA, 1992.

Table 1: Results for despeckling of simulated image "Lena", obtained on different number of looks by means of various filter, in the case of IF and SIF.

L	filter	PSNR		MSSIM		$\mu_{\hat{u}}$		$\sigma^2_{\hat{u}} \cdot L$	
		IF	SIF	IF	SIF	IF	SIF	IF	SIF
1	noisy	11.30		0.109		-		-	
	LMMSE	24.55	24.69	0.513	0.524	0.90	0.89	0.639	0.619
	MAP–GG	26.32	26.90	0.736	0.735	0.98	0.98	0.998	0.938
	MAP–GG–S	26.33	26.87	0.736	0.734	0.98	0.98	0.999	0.937
	MAP–LG	26.16	26.67	0.725	0.718	0.95	0.96	0.874	0.875
	MAP–LG–S	26.17	26.66	0.725	0.718	0.95	0.96	0.874	0.874
2	noisy	14.46		0.175		-		-	
	LMMSE	26.65	26.95	0.630	0.635	0.93	0.94	0.666	0.661
	MAP–GG	28.03	28.74	0.785	0.787	0.99	0.98	1.037	0.935
	MAP–GG–S	28.06	28.71	0.785	0.786	0.99	0.98	1.014	0.933
	MAP–LG	27.82	28.48	0.775	0.772	0.97	0.97	0.885	0.887
	MAP–LG–S	27.86	28.50	0.775	0.772	0.97	0.97	0.888	0.886
4	noisy	17.55		0.258		-		-	
	LMMSE	28.53	28.98	0.720	0.725	0.96	0.96	0.678	0.683
	MAP–GG	29.64	30.34	0.824	0.824	0.99	0.99	1.085	0.938
	MAP–GG–S	29.71	30.32	0.825	0.824	0.99	0.99	1.041	0.933
	MAP–LG	29.38	30.10	0.814	0.815	0.97	0.98	0.899	0.901
	MAP–LG–S	29.50	30.19	0.816	0.817	0.98	0.98	0.914	0.895
16	noisy	23.68		0.468		-		-	
	LMMSE	32.55	32.95	0.850	0.852	0.98	0.99	0.672	0.668
	MAP–GG	33.13	33.70	0.883	0.886	1.00	0.99	1.066	0.917
	MAP–GG–S	33.16	33.64	0.881	0.884	1.00	0.99	1.021	0.892
	MAP–LG	32.89	33.52	0.880	0.883	0.99	0.99	0.926	0.894
	MAP–LG–S	33.18	33.66	0.882	0.883	0.99	0.99	0.989	0.869

Table 2: Results for despeckling of simulated image "Barbara", obtained on different number of looks by means of various filter, in the case of IF and SIF.

L	filter	PSNR		MSSIM		$\mu_{\hat{u}}$		$\sigma^2_{\hat{u}} \cdot L$	
		IF	SIF	IF	SIF	IF	SIF	IF	SIF
1	noisy	11.52		0.181		-		-	
	LMMSE	22.61	22.85	0.518	0.548	0.88	0.88	0.633	0.593
	MAP–GG	22.89	23.51	0.606	0.640	0.98	0.97	1.198	0.969
	MAP–GG–S	23.05	23.70	0.617	0.653	0.98	0.97	1.190	0.953
	MAP–LG	22.89	23.44	0.603	0.631	0.94	0.96	0.903	0.883
	MAP–LG–S	23.00	23.59	0.610	0.640	0.94	0.95	0.897	0.874
2	noisy	14.68		0.280		-		-	
	LMMSE	24.33	24.68	0.634	0.657	0.92	0.92	0.636	0.624
	MAP–GG	24.42	25.11	0.691	0.720	0.98	0.97	1.220	0.929
	MAP–GG–S	24.79	25.38	0.707	0.734	0.98	0.97	1.172	0.909
	MAP–LG	24.17	24.89	0.680	0.709	0.95	0.96	0.883	0.879
	MAP–LG–S	24.56	25.18	0.696	0.722	0.95	0.96	0.870	0.863
4	noisy	17.80		0.397		-		-	
	LMMSE	26.17	26.56	0.737	0.754	0.94	0.95	0.637	0.630
	MAP–GG	26.31	26.92	0.777	0.794	0.99	0.98	1.215	0.897
	MAP–GG–S	26.64	27.18	0.792	0.806	0.99	0.98	1.321	0.872
	MAP–LG	25.86	26.59	0.762	0.783	0.96	0.97	0.878	0.868
	MAP–LG–S	26.30	26.96	0.780	0.797	0.97	0.97	0.941	0.844
16	noisy	23.93		0.630		-		-	
	LMMSE	30.21	30.55	0.873	0.878	0.98	0.98	0.610	0.581
	MAP–GG	30.35	30.86	0.886	0.892	0.99	0.99	1.052	0.826
	MAP–GG–S	30.30	30.84	0.890	0.895	1.00	0.99	1.149	0.778
	MAP–LG	29.93	30.55	0.879	0.887	0.98	0.99	0.879	0.819
	MAP–LG–S	30.35	30.84	0.888	0.893	0.99	0.99	0.955	0.765

Table 3: Results for despeckling of simulated image "San Francisco", obtained on different number of looks by means of various filter, in the case of IF and SIF.

L	filter	PSNR		MSSIM		$\mu_{\hat{u}}$		$\sigma^2_{\hat{u}} \cdot L$	
		IF	SIF	IF	SIF	IF	SIF	IF	SIF
1	noisy	15.23		0.194		-		-	
	LMMSE	23.94	24.58	0.573	0.588	0.88	0.88	0.655	0.620
	MAP–GG	23.99	24.90	0.623	0.646	0.98	0.98	1.184	1.009
	MAP–GG–S	24.03	24.89	0.624	0.646	0.98	0.98	1.128	1.002
	MAP–LG	24.00	24.87	0.624	0.645	0.94	0.96	0.919	0.917
	MAP–LG–S	24.03	24.89	0.624	0.645	0.94	0.96	0.919	0.915
2	noisy	18.42		0.303		-		-	
	LMMSE	25.47	26.23	0.658	0.675	0.92	0.92	0.668	0.647
	MAP–GG	25.27	26.28	0.672	0.695	0.99	0.98	1.379	0.983
	MAP–GG–S	25.35	26.28	0.674	0.695	0.99	0.98	1.517	0.972
	MAP–LG	25.27	26.25	0.674	0.695	0.95	0.97	0.921	0.915
	MAP–LG–S	25.39	26.34	0.677	0.697	0.96	0.97	0.961	0.908
4	noisy	21.53		0.435		-		-	
	LMMSE	27.07	27.84	0.727	0.741	0.94	0.95	0.673	0.646
	MAP–GG	26.71	27.73	0.719	0.738	1.00	0.99	2.226	0.972
	MAP–GG–S	26.88	27.79	0.722	0.739	1.00	0.98	1.652	0.947
	MAP–LG	26.67	27.70	0.721	0.740	0.96	0.98	0.955	0.923
	MAP–LG–S	26.92	27.86	0.726	0.743	0.98	0.98	1.446	0.901
16	noisy	27.66		0.716		-		-	
	LMMSE	30.80	31.36	0.840	0.846	0.97	0.98	0.611	0.544
	MAP–GG	30.39	31.10	0.813	0.822	1.00	0.99	1.633	0.884
	MAP–GG–S	30.35	30.86	0.813	0.822	1.00	0.99	1.102	0.762
	MAP–LG	30.24	31.12	0.818	0.827	0.98	0.99	1.039	0.868
	MAP–LG–S	30.69	31.22	0.824	0.830	0.99	0.99	1.197	0.772

Table 4: Results for despeckling of simulated image "Lena", obtained on different number of looks by means of various filter, in the case of AF.

L	filter	PSNR	MSSIM	$\mu_{\hat{u}}$	$\sigma^2_{\hat{u}} \cdot \frac{\pi L}{4-\pi}$
1	noisy	11.27	0.109	-	-
	LMMSE	24.67	0.520	0.97	0.744
	MAP–GG	26.92	0.736	0.99	0.969
	MAP–GG–S	26.88	0.735	0.99	0.968
	MAP–LG	26.68	0.717	0.99	0.937
	MAP–LG–S	26.67	0.717	0.99	0.936
2	noisy	14.29	0.170	-	-
	LMMSE	26.79	0.628	0.98	0.739
	MAP–GG	28.55	0.781	0.99	0.957
	MAP–GG–S	28.52	0.781	0.99	0.955
	MAP–LG	28.30	0.766	0.99	0.928
	MAP–LG–S	28.31	0.767	0.99	0.927
4	noisy	17.31	0.252	-	-
	LMMSE	28.89	0.722	0.99	0.728
	MAP–GG	30.29	0.825	1.00	0.949
	MAP–GG–S	30.25	0.824	0.99	0.945
	MAP–LG	30.04	0.815	0.99	0.924
	MAP–LG–S	30.12	0.816	0.99	0.919
16	noisy	23.31	0.455	-	-
	LMMSE	32.74	0.847	1.00	0.684
	MAP–GG	33.52	0.883	1.00	0.926
	MAP–GG–S	33.46	0.881	1.00	0.902
	MAP–LG	33.35	0.880	1.00	0.908
	MAP–LG–S	33.49	0.880	1.00	0.882

Table 5: Results for despeckling of simulated image "Barbara", obtained on different number of looks by means of various filter, in the case of AF.

L	filter	PSNR	MSSIM	$\mu_{\hat{u}}$	$\sigma^2_{\hat{u}} \cdot \frac{\pi L}{4-\pi}$
1	noisy	11.54	0.180	-	-
	LMMSE	22.83	0.548	0.96	0.722
	MAP–GG	23.50	0.641	0.99	0.980
	MAP–GG–S	23.68	0.653	0.99	0.969
	MAP–LG	23.40	0.632	0.98	0.939
	MAP–LG–S	23.56	0.641	0.98	0.933
2	noisy	14.54	0.276	-	-
	LMMSE	24.65	0.659	0.97	0.708
	MAP–GG	25.06	0.720	0.99	0.955
	MAP–GG–S	25.36	0.734	0.99	0.938
	MAP–LG	24.83	0.708	0.98	0.926
	MAP–LG–S	25.15	0.722	0.98	0.912
4	noisy	17.55	0.388	-	-
	LMMSE	26.44	0.746	0.98	0.685
	MAP–GG	26.77	0.788	0.99	0.929
	MAP–GG–S	27.04	0.801	0.99	0.904
	MAP–LG	26.45	0.777	0.99	0.911
	MAP–LG–S	26.81	0.791	0.99	0.885
16	noisy	23.57	0.617	-	-
	LMMSE	30.32	0.873	0.99	0.602
	MAP–GG	30.65	0.888	1.00	0.842
	MAP–GG–S	30.63	0.892	1.00	0.795
	MAP–LG	30.32	0.883	0.99	0.841
	MAP–LG–S	30.62	0.890	1.00	0.784

Table 6: Results for despeckling of simulated image "San Francisco", obtained on different number of looks by means of various filter, in the case of AF.

L	filter	PSNR	MSSIM	$\mu_{\hat{u}}$	$\sigma^2_{\hat{u}} \cdot \frac{\pi L}{4-\pi}$
1	noisy	15.23	0.194	-	-
	LMMSE	24.67	0.594	0.96	0.740
	MAP–GG	24.97	0.648	0.99	0.988
	MAP–GG–S	24.98	0.648	0.99	0.985
	MAP–LG	24.93	0.646	0.98	0.948
	MAP–LG–S	24.96	0.647	0.98	0.947
2	noisy	18.26	0.297	-	-
	LMMSE	26.14	0.672	0.97	0.727
	MAP–GG	26.19	0.692	0.99	0.991
	MAP–GG–S	26.23	0.693	0.99	0.981
	MAP–LG	26.15	0.692	0.99	0.953
	MAP–LG–S	26.24	0.694	0.99	0.945
4	noisy	21.29	0.426	-	-
	LMMSE	27.77	0.739	0.98	0.700
	MAP–GG	27.66	0.736	0.99	0.986
	MAP–GG–S	27.69	0.737	0.99	0.962
	MAP–LG	27.63	0.738	0.99	0.953
	MAP–LG–S	27.78	0.741	0.99	0.930
16	noisy	27.30	0.702	-	-
	LMMSE	31.13	0.841	0.99	0.578
	MAP–GG	30.85	0.816	1.00	0.913
	MAP–GG–S	30.68	0.818	1.00	0.801
	MAP–LG	30.88	0.821	0.99	0.901
	MAP–LG–S	31.00	0.825	1.00	0.808

Table 7: Statistical parameters derived from 1-look (CS–1L) and 4-look intensity (CS–4L) COSMO-SkyMed images despeckled by means of various filter.

image	filter	Zone A				Zone B			
		$\mu_{\hat{u}}$		$\sigma^2_{\hat{u}} \cdot L$		$\mu_{\hat{u}}$		$\sigma^2_{\hat{u}} \cdot L$	
		IF	SIF	IF	SIF	IF	SIF	IF	SIF
CS–1L	LMMSE	0.92	0.91	0.661	0.627	0.91	0.90	0.630	0.606
	MAP–GG	0.99	0.99	0.980	0.954	0.98	0.98	0.935	0.918
	MAP–GG–S	0.99	0.99	0.980	0.954	0.98	0.98	0.935	0.918
	MAP–LG	0.98	0.98	0.912	0.890	0.96	0.97	0.868	0.859
	MAP–LG–S	0.98	0.98	0.912	0.890	0.96	0.97	0.868	0.859
CS–4L	LMMSE	0.95	0.96	0.726	0.721	0.95	0.96	0.701	0.706
	MAP–GG	0.99	1.00	1.280	1.170	0.99	1.00	1.143	1.117
	MAP–GG–S	0.99	1.00	1.269	1.156	0.99	1.00	1.143	1.117
	MAP–LG	0.98	0.99	1.078	1.085	0.98	0.99	1.034	1.045
	MAP–LG–S	0.98	0.99	1.073	1.079	0.98	0.99	1.034	1.045

Table 8: Statistical parameters derived from 4-look amplitude (CS–4L–AF) COSMO-SkyMed images despeckled by means of various filter.

image	filter	Zone A		Zone B	
		$\mu_{\hat{u}}$	$\sigma^2_{\hat{u}} \cdot L$	$\mu_{\hat{u}}$	$\sigma^2_{\hat{u}} \cdot \frac{\pi L}{4-\pi}$
CS–4L–AF	LMMSE	0.99	0.731	0.99	0.736
	MAP–GG	1.00	1.140	1.00	1.121
	MAP–GG–S	1.00	1.127	1.00	1.121
	MAP–LG	0.99	1.062	0.99	1.068
	MAP–LG–S	0.99	1.057	0.99	1.069